High mobility two-dimensional electron gases in nitride heterostructures with high Al composition AlGaN alloy barriers

Guowang Li, Yu Cao, Huili Grace Xing, and Debdeep Jena[a)]
Department of Electrical Engineering, University of Notre Dame, Indiana 46556, USA

(Received 22 October 2010; accepted 11 November 2010; published online 1 December 2010)

We report high-electron mobility nitride heterostructures with >70% Al composition AlGaN alloy barriers grown by molecular beam epitaxy. Direct growth of such AlGaN layers on GaN resulted in hexagonal trenches and a low mobility polarization-induced charge. By applying growth interruption at the heterojunction, the surface morphology improved dramatically and the room temperature two-dimensional electron gas (2DEG) mobility increased by an order of magnitude, exceeding 1300 $cm^2/V\,s$. The 2DEG density was tunable at $0.4–3.7\times10^{13}/cm^2$ by varying the total barrier thickness (t). Surface barrier heights of the heterostructures were extracted and exhibited dependence on t. © *2010 American Institute of Physics*. [doi:10.1063/1.3523358]

Binary AlN barriers have enabled excellent transport properties of two-dimensional electron gases (2DEG) in nitride heterostructures.[1,2] However, low contact resistance is hampered by the wide band gap (6.2 eV) of AlN.[3] The contact resistance could be lowered by adding Ga to AlN to form AlGaN ternary alloy and reducing the band gap. In low Al composition (<40%) AlGaN/GaN high-electron mobility transistor (HEMT) technology, enormous progress has already been achieved in high power and high frequency applications.[4] For radio frequency (rf) electronics, the lateral scaling of gate lengths down to deep submicrometer dimensions to boost rf performance needs to be accompanied by a vertical scaling of barrier thickness. This requires high Al composition AlGaN to maintain a 2DEG density and low sheet resistance.[5] The alloy scattering rate is given by $1/\tau_m^{alloy} \propto (\Delta E_C)^2 x(1-x) P_b^2$, where x is the Al composition, $\Delta E_C = (E_C^{AlN} - E_C^{GaN})$ is the conduction band offset between AlN and GaN, and P_b is the integrated probability of finding the electron in the barrier region.[6] Comparing alloy scattering due to AlGaN alloy barriers with $x=72\%$ and $x=28\%$, since the factor $(\Delta E_C)^2 x(1-x)$ is identical for both, scattering is suppressed in the $x=72\%$ barrier due to lower wave function penetration. Compared to lattice-matched InAlN barriers,[7] lower gate tunneling current is expected in high Al composition AlGaN barriers due to their higher band gap and conduction band offset. Also for optoelectronics, AlGaN-based deep UV light emitters require high Al composition.

Epitaxial growth of high Al composition (>50%) films has been demonstrated by metalorganic chemical vapor deposition.[8–10] The 2DEG electron mobility at room temperature (RT) is limited to $\sim500\ cm^2/V\,s$ with Al composition higher than 70%,[8] which holds back reasonable device performance. In molecular beam epitaxy (MBE) growth, the low surface mobility of Al atoms severely limits the AlGaN epilayer quality. Spontaneous compositional modulation is observed in MBE-grown materials.[11,12] A method that suppresses the compositional modulation and results in high mobility is desirable. In this work, we report such a method and demonstrate HEMT structures with >70% AlGaN alloy barriers and high RT carrier mobility ($\sim1350\ cm^2/V\,s$). These structures have been recently used to fabricate HEMTs that were reported elsewhere.[13]

All the nitride heterostructures were grown on semi-insulating GaN templates on sapphire by MBE in a Veeco Gen 930 system, Veeco MBE Systems, 4900 Constellation Drive, St. Paul, MN 55127. A Veeco rf source was used to supply active nitrogen. An ultrathin (~1.5 nm) AlN nucleation layer was grown in the N-rich regime to remove buffer leakage using a polarization-dipole induced back barrier,[14] followed by a ~200-nm-thick unintentionally doped GaN buffer, and barrier cap layers. Hall-effect measurements were performed on all samples at RT and 77 K. In dots were used to form Ohmic contacts to the 2DEG at the heterojunctions.

Growths were performed in the metal-rich regime with fluxes of $F_{Ga} \sim (1.1–1.3)\times10^{-7}$ Torr, $F_{Al} \sim 4.3\times10^{-8}$ Torr, rf power of 275 W, and growth temperature $T_{Gr} \sim (640–740)\,^{\circ}C$. The epitaxial growth of relatively thick (>3 nm) high Al composition (>70%) AlGaN alloy layer directly on GaN always resulted in hexagonal trenched surface morphologies, as shown in the atomic force microscopy (AFM) scans in Figs. 1(a) and 1(b). The hexagonal trenches were centered at bright spots, which may be related to the threading dislocations (TDs) with screw components.[15] Hexagonal trenches are clearly resolved in Fig. 1(a) with a TD density of $\sim10^8\ cm^{-2}$ and merge with each other with higher TD density of $\sim10^9\ cm^{-2}$ in Fig. 1(b). The corresponding root-mean-square (rms) roughness for $2\times2\ \mu m^2$ scan was higher than 0.5 nm. The lower mobility of Al adatoms on the growth surface in comparison with Ga adatoms may induce spontaneous lateral thickness and possible phase modulation, resulting in the clear hexagonal trenches. The AlGaN barrier layer was split into hexagonal trenches deeper than the barrier thickness, causing the conducting polarization-induced 2DEG channel to be separated into partially connected regions. This effect prevented electrons to flow smoothly and was independent of temperature. As a result, the RT electron mobility was severely affected and limited to below $\sim150\ cm^2/V\,s$, and there was no evident increase in mobility at 77 K, as shown in Fig. 3(a). The 2DEG densities of such samples without the AlN interlayer varied over a large range as the growth conditions were changed, as shown in Fig. 3(b). The RT and 77 K sheet

a)Electronic mail: djena@nd.edu.

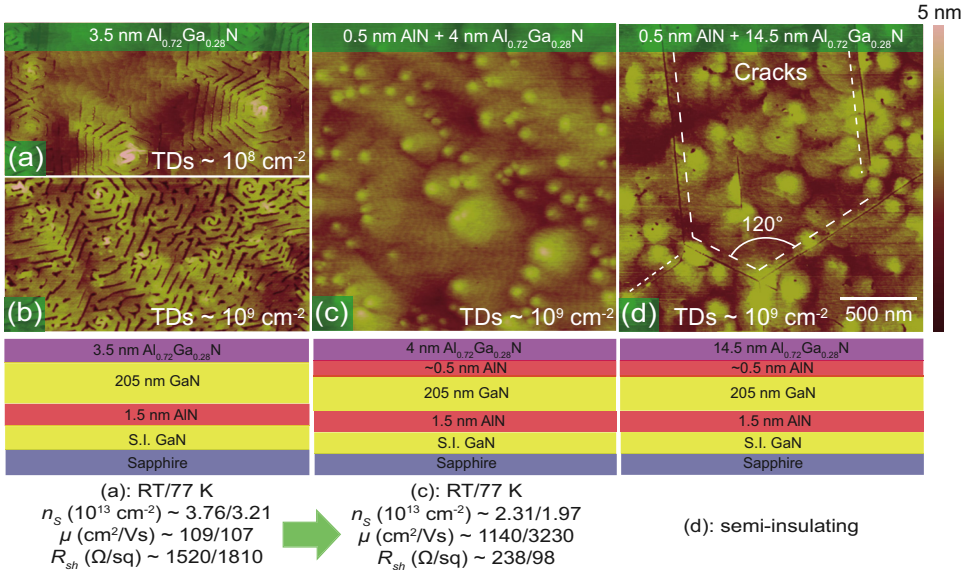

FIG. 1. (Color online) Comparison of 2×2 μm^2 AFM scan images of as-grown AlGaN surface: [(a) and (b)] w/o AlN interlayer and [(c) and (d)] w/AlN interlayer. TD densities are $\sim10^8$ cm^{-2} in (a) and $\sim10^9$ cm^{-2} in (b), (c), and (d), respectively. In (d), cracks are shown clearly in a 15 nm barrier sample. Corresponding schematic layer structures and Hall-effect measurement results at RT and 77 K are shown also.

resistance (R_{sh}) were typically in the range from 1000 to 2500 $\Omega/\square$.

To suppress the formation of the hexagonal trenches, various growth conditions were explored (growth temperatures at 640–740 °C, various metal fluxes, and metal-to-nitrogen rich growth regimes) but did not result in high-electron mobilities. Then, the growth was interrupted at the heterointerface to insert a few monolayers of AlN at the AlGaN/GaN interface. As a result, the surface morphology was dramatically modified and consisted of terraced atomic steps, as shown in Fig. 1(c). High-resolution transmission electron microscopy images (not shown here) indicated the existence of one to two AlN monolayer(s) at the interface. Hereafter, samples with AlN interlayers refer to those grown by applying the quasigrowth interruption technology, and samples without AlN interlayers refer to those with AlGaN layers directly on GaN. All growths of the samples with AlN interlayers were performed in the metal-rich regime, with $F_{Ga}\sim1.3\times10^{-7}$ Torr, $F_{Al}\sim4.3\times10^{-8}$ Torr, rf power of 275 W, and $T_{Gr}\sim720$ °C. The AlN interlayer resulted in a markedly different nucleation surface for AlGaN than the GaN buffer and thus enabled the MBE growth of high quality >70% Al composition AlGaN layers with rms roughness of ~0.4 nm for the 2×2 μm^2 scans. Moreover, the AlN interlayer improved the carrier mobility by removing the alloy scattering. For $Al_{0.72}Ga_{0.28}N$ layer coherently strained on GaN, the misfit strain is $\epsilon\sim1.7\%$. The critical thickness of $Al_{0.72}Ga_{0.28}N$ on GaN is roughly estimated to be $t_{cr}\sim b_e/2\epsilon\sim9.2$ nm, where $b_e=0.3189$ nm is the Burgers' vector length.[16] Figure 1(d) shows very clear cracks along the hexagonal axes with ~15-nm-thick barrier. The crack lines are associated with the tips of threading dislocations and propagate along cleavage planes.

The growth rate and Al composition of the AlGaN barrier layers were calibrated by high-resolution x-ray diffraction (XRD) measurements on several multiple quantum well calibration structures. Based on the calibration, the AlN layer thicknesses were kept around 0.5 nm for all the samples with AlN interlayers. The high-resolution XRD ω-2θ scan measured for a 9.5 nm $Al_{0.72}Ga_{0.28}N$/0.5 nm AlN barrier heterostructure is shown in Fig. 2, along with a simulated model. The high Al composition AlGaN peak is clearly resolved to the right of the main GaN (0002) peak. Interference fringes due to the AlN nucleation layer underneath the GaN buffer layer are also clearly resolved, providing an accurate measurement of the GaN buffer layer thickness and proving the existence of the AlN nucleation layer at the regrowth interface. The corresponding schematic of the sample structures and 2×2 μm^2 AFM scan image are shown in the insets of Fig. 2. Though the barrier thickness of ~10 nm is close to t_{cr}, no evident cracks are observed.

For the samples with AlN interlayers, the RT mobilities were improved by one order of magnitude compared to those without AlN interlayers, as shown in Fig. 3(a). The RT and 77 K mobilities were ~1200 and ~3000 cm^2/V s, respectively, for $t\sim3$–4.5 nm, where t was the total barrier thickness [AlN(~0.5 nm)+AlGaN]. With a 3.5 nm barrier, RT/77 K mobilities reached 1350/3610 cm^2/V s, respectively. The 77 K mobility was affected mainly by interface roughness scattering, while RT mobility was limited by polar optical phonons.[2] With $t\geq5.5$ nm, enhanced interface roughness scattering and possible strain relaxation reduced the 2DEG mobility. As shown in Fig. 3(b), the polarization-induced RT 2DEG density increased from $\sim4\times10^{12}/cm^2$ to $\sim3.7\times10^{13}/cm^2$, with t increasing from 2.5 to 8 nm. Although for samples with AlN interlayers the 2DEG density

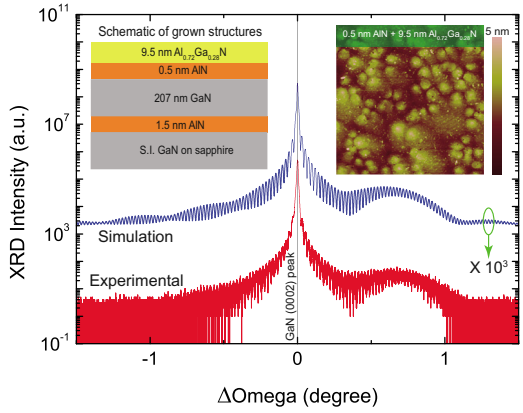

FIG. 2. (Color online) High-resolution x-ray diffraction ω-2θ measurement on a HEMT structure with a 10 nm barrier. Inset: corresponding schematics of the grown structure and a 2×2 μm^2 AFM scan image.

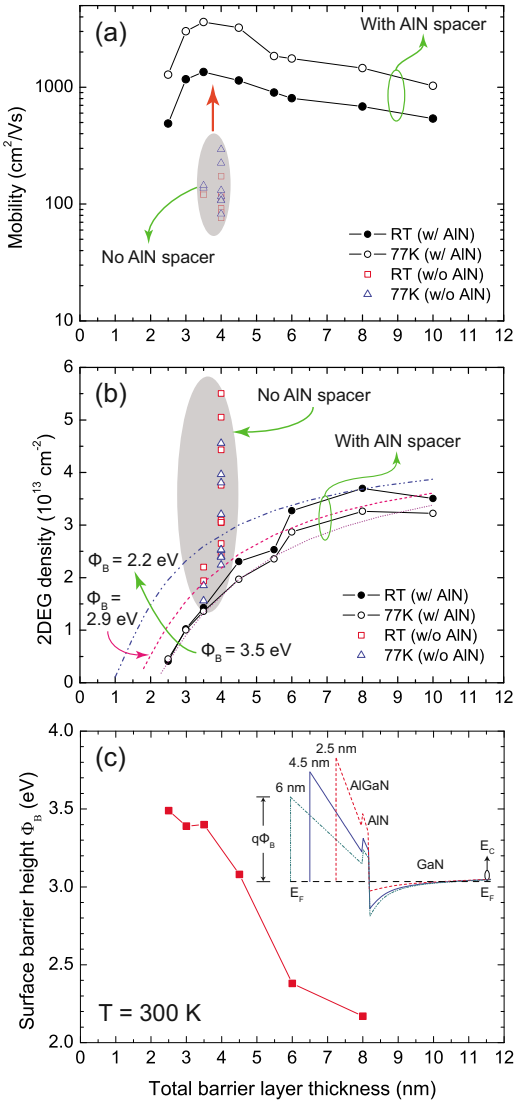

FIG. 3. (Color online) (a) Dependence of RT and 77 K mobilities on the total barrier thickness (t) w/ and w/o AlN interlayers. (b) 2DEG densities measured at RT and 77 K with different t w/ and w/o AlN interlayers; different surface barrier heights (Φ_B) of 2.2, 2.9, and 3.5 eV were used in self-consistent Poisson–Schrodinger simulation of heterostructures with AlN interlayers to predict the trend of RT 2DEG density. (c) Extracted Φ_B from RT 2DEG densities w/AlN interlayers; inset: schematic energy band diagrams showing dependence of Φ_B on t, where E_C is the conduction band, E_F is the Fermi level, and q is the electron charge.

kept increasing with $t \geq 5.5$ nm, the decreasing mobility resulted in no reduction in sheet resistance. At $t=4.5$ nm, the minimum R_{sh} value of RT/77 K was 240/98 $\Omega/\square$, respectively. The heterostructures with AlN interlayers were modeled using a self-consistent Poisson–Schrödinger solver.[17] Different fixed surface barrier heights (Φ_B) of 2.2, 2.9, and 3.5 eV were used in the simulation, and the results are shown in Fig. 3(b). It is evident that a fixed Φ_B cannot explain the experimental data well over the entire range of barrier thicknesses. In low Al composition AlGaN barriers, the surface barrier height Φ_B was recently observed to be dependent on carrier concentration.[18] For $Al_{0.72}Ga_{0.28}N$ barriers, different surface barrier heights were extracted from the measured RT 2DEG densities of different barrier thicknesses by solving Poisson–Schrödinger equations. As shown in Fig. 3(c), the extracted Φ_B decreases with increasing 2DEG density. The schematic energy band diagrams with $t=2.5$, 4.5, and 6 nm are shown in the inset. With increasing t, the strength of the dipole formed by the 2DEG and the surface charge increases and screens more of the fixed polarization dipole, resulting in a smaller electric field in the barrier layer. The unpinned surface Fermi level in wide band gap AlGaN layers is very attractive for employing work function engineering to tune threshold voltages of transistors.[13]

In conclusion, we have succeeded in demonstrating that carrier mobility can reach up to 1350 $cm^2/V\,s$ at room temperature in HEMT structures with $Al_{0.72}Ga_{0.28}N$ alloy barriers. With a total barrier thickness of 4.5 nm, RT sheet resistance can be as low as 240 $\Omega/\square$. Direct epitaxial growth of thin barrier high Al composition (>70%) AlGaN layers on GaN resulted in hexagonal trenches, which split the conducting 2DEG channels and hampered the motion of electrons, and the RT electron mobility was limited to ~300 $cm^2/V\,s$. An ultrathin (~0.5 nm) AlN interlayer induced by the quasi-growth interruption technology was crucial to suppress hexagonal trench formation and improved mobilities by more than one order of magnitude. The finding paves the way for exploring deep submicron HEMTs with high Al composition AlGaN barriers and also provides a MBE growth technology suitable for deep UV light emitters.

[1] I. P. Smorchkova, S. Keller, S. Heikman, C. R. Elsass, B. Heying, P. Fini, J. Speck, and U. K. Mishra, Appl. Phys. Lett. **77**, 3998 (2000).
[2] Y. Cao and D. Jena, Appl. Phys. Lett. **90**, 182112 (2007).
[3] T. Zimmermann, D. Deen, Y. Cao, D. Jena, and H. Xing, Phys. Status Solidi C **5**, 2030 (2008).
[4] U. K. Mishra, L. Shen, T. E. Kazior, and Y. F. Wu, Proc. IEEE **96**, 287 (2008).
[5] Y. Pei, R. Chu, L. Shen, N. A. Fichtenbaum, Z. Chen, D. Brown, S. Keller, S. P. Denbaars, and U. K. Mishra, IEEE Electron Device Lett. **29**, 300 (2008).
[6] G. Bastard, *Wave Mechanics Applied to Semiconductor Heterostructures* (Les Éditions de Physique, Les Ulis Cedex, France, 1988).
[7] R. Buttè, J.-F. Carlin, E. Feltin, M. Gonschorek, S. Nicolay, G. Christmann, D. Simeonov, A. Castiglia, J. Dorsaz, H. J. Buehlmann, S. Christopoulos, G. Baldassarri Höger von Högersthal, A. J. D. Grundy, M. Mosca, C. Pinquier, M. A. Py, F. Demangeot, J. Frandon, P. G. Lagoudakis, J. J. Baumberg, and N. Grandjean, J. Phys. D: Appl. Phys. **40**, 6328 (2007).
[8] M. Miyoshi, M. Sakai, H. Ishikawa, T. Egawa, T. Jimbo, M. Tanaka, and O. Oda, J. Cryst. Growth **272**, 293 (2004).
[9] S. Heikman, S. Keller, S. Newman, Y. Wu, C. Moe, B. Moran, M. Schmidt, U. K. Mishra, J. S. Speck, and S. P. DenBaars, Jpn. J. Appl. Phys., Part 2 **44**, L405 (2005).
[10] H. Hirayama, T. Yatable, N. Noguxhi, T. Ohashi, and N. Kamata, Appl. Phys. Express **1**, 051101 (2008).
[11] E. Iliopoulos, K. F. Ludwig, Jr., T. D. Moustakas, and S. N. G. Chu, Appl. Phys. Lett. **78**, 463 (2001).
[12] M. Gao, S. T. Bradley, Y. Cao, D. Jena, Y. Lin, S. A. Ringel, J. Hwang, W. J. Schaff, and L. J. Brillson, J. Appl. Phys. **100**, 103512 (2006).
[13] G. Li, T. Zimmermann, Y. Cao, C. Lian, X. Xing, R. Wang, P. Fay, H. Xing, and D. Jena, IEEE Electron Device Lett. **31**, 954 (2010).
[14] Y. Cao, T. Zimmermann, H. Xing, and D. Jena, Appl. Phys. Lett. **96**, 042102 (2010).
[15] B. Heying, E. J. Tarsa, C. R. Elsass, P. Fini, S. P. DenBaars, and J. S. Speck, J. Appl. Phys. **85**, 6470 (1999).
[16] J. Singh, *Physics of Semiconductors and Their Heterostructures* (McGraw-Hill, New York, 1992), p. 734.
[17] I. H. Tan, G. L. Snider, L. D. Chang, and E. L. Hu, J. Appl. Phys. **68**, 4071 (1990).
[18] K. Köhler, S. Müller, R. Aidam, P. Waltereit, W. Pletschen, L. Kirste, H. P. Menner, W. Bronner, A. Leuther, R. Quay, M. Mikulla, O. Ambacher, R. Granzner, F. Schwierz, C. Buchheim, and R. Goldhahn, J. Appl. Phys. **107**, 053711 (2010).